Contents lists available at ScienceDirect

# Atmospheric Research

# The role of atmospheric aerosols on severe convective precipitation in a Mediterranean coastal region

Francesco Ferrari [a,f,*], Umberto Rizza [b], Mauro Morichetti [b], Federico Cassola [c], Mario Marcello Miglietta [d,e], Andrea Mazzino [a,f]

[a] Dipartimento di Ingegneria Civile, Chimica e Ambientale, University of Genova, Via Montallegro 1, 16145 Genova, Italy
[b] National Research Council—Institute of Atmospheric Sciences and Climate (CNR-ISAC), 73100 Lecce, Italy
[c] Agenzia Regionale per la Protezione dell'Ambiente Ligure, Viale Brigate Partigiane 2, 16129 Genova, Italy
[d] Department of Earth and Geoenvironmental Sciences, University of Bari "Aldo Moro", Via Orabona 4, 70125 Bari, Italy
[e] National Research Council of Italy - Institute of Atmospheric Sciences and Climate (CNR-ISAC), Corso Stati Uniti, 4 - 35127 Padua, Italy
[f] Istituto Nazionale di Fisica Nucleare, Genova Section, Via Dodecaneso 33, 16146 Genova, Italy

## ARTICLE INFO

## ABSTRACT

Liguria, located in the Northwest of Italy, is one of the Italian regions hit in the recent past by some of the most severe precipitation events among the ones observed in Italy. From a synoptic point of view, similar configurations characterize the extreme events that affected Liguria, i.e. the simultaneous presence of a deep pressure minimum west of the region and a strong high pressure over eastern Europe. Such conditions are favorable to the triggering of a quasi-stationary mesoscale V-shaped convective system over the Ligurian Sea. Furthermore, this kind of configuration is favorable to the formation and intrusion of wide plumes of aerosol, mainly mineral dust from the Sahara Desert and sea salt aerosols generated under high wind conditions in the Mediterranean basin. The present study aims at evaluating the impact that these aerosol plumes can have on meteorological fields during the triggering and evolution of the deep convective systems responsible for the Liguria flooding events. This study is carried out through numerical simulations performed with the WRF-Chem model, version 4.0. In particular, our main aim is to investigate the influence that the so-called direct (aerosol-radiation) and indirect (aerosol-cloud) interactions may have on mesoscale V-shape convective systems and on the associated rainfall events. In the simulations in which the direct aerosol effects are switched on, a consistent weakening signal is identified in the wind speed in all simulations; a major role seems to be played by the increase of downward longwave radiation in the presence of aerosol, that, by reducing the land-sea temperature gradient, causes the weakening of surface winds. More complex are the consequences of aerosol on the amount/intensity of the resulting precipitations. Unexpectedly, a reduced convergence is not necessarily associated with a weakening of precipitation and in half of the studied cases the interaction between aerosol, moisture and radiation increases the instability despite the reduced dynamical forcing due to the weakening of the convergence.

## 1. Introduction

More than 2 billion people worldwide were affected by floods in the last twenty years, a number that continues to climb as occurrences of major flood events become more frequent and severe. In particular, the Mediterranean region is a nearly enclosed basin surrounded by complex orography close to the coast, making the area particularly prone to events related to the water cycle. During the years, many research programs, such as the Hydrological cycle in the Mediterranean eXperiment (HyMeX, http://www.hymex.org, accessed on 20 May 2023), have

been developed to monitor, analyze, and model the regional hydrometeorological cycle in the region (Drobinski et al., 2014). In the middle of the Mediterranean basin, the Italian peninsula, that extends from the southern Alps in the north to the central Mediterranean Sea in the south, is particularly exposed to natural hazards associated with severe precipitation (Miglietta and Davolio, 2022). Liguria, located in the Northwest of Italy, is one of the Italian regions hit in the recent past by some of the most severe precipitation events among those occurred in Italy. This region is thus a natural laboratory for a better understanding of the ruling mechanisms at the origin of extreme precipitation events.

Quasi-stationary mesoscale convective systems, responsible for the majority of extreme precipitation events that may occasionally affect this area during Autumn, share a common synoptic configuration. When a low pressure minimum approaches the western Mediterranean coast, it usually triggers intense southerly, warm and moist flows over the Tyrrhenian Sea and a cooler shallow flow from the Po valley towards the Ligurian coast. The interaction between these two different flows can lead to the formation of convergence lines resulting in the development of severe self-generating, V-shaped convective systems able to produce devastating precipitation over small areas (Cassola et al., 2023).

The synoptic settings leading to heavy precipitation events are well known; however, an accurate description and simulation of the mechanisms and processes that rule the initiation and localization of these precipitation systems, especially when convection dominates, is still challenging. The complex multi-scale interaction among the moist ambient inflow, extracting moisture and heat from the sea surface, deep convection, and topography make the precise prediction of the location, timing and amount of precipitation associated with these systems a daunting task (Cavaleri et al., 2022; Miglietta and Davolio, 2022).

A further ingredient which may play a role in triggering, reinforcing or attenuating these events is represented by aerosols. Indeed, due to the proximity of Southern Europe to the Sahara desert, under the proper synoptic conditions the central Mediterranean basin can be affected by more or less extensive Saharan dust plumes. The synoptic setting conducive to extreme events on the Ligurian basin is also responsible for the arrival of large amounts of aerosols over Northern Italy. In particular, all most recent Ligurian floods have been accompanied by extensive dust plumes coming from Northern Africa (Rizza et al., 2017) and further enriched by sea spray during their journey over the Mediterranean Sea.

Hence, the main focus of the present work is to study the role of the aerosols in triggering and determining the evolution of Ligurian deep convective V-shaped, flood-causing, events that are responsible for all major floods happened in Liguria in the last decades. This will be realized by activating the so-called direct aerosol-radiation interactions (Charlson et al., 1992; Kiehl and Briegleb, 1993; Xie et al., 2013; Rizza et al., 2023) and indirect aerosol-cloud interactions (Twomey, 1974; Twomey, 1991; Huang et al., 2014; Duan et al., 2019) in the Weather Research and Forecasting coupled with Chemistry (WRF-Chem) model (Grell et al., 2005).

Some preceding papers studied the impact of dust on mesoscale phenomena; among them, we mention Kumar et al. (2014), who used the WRF-Chem model to study the effect of dust plumes on the typical pre-monsoon conditions in northern India; Liu et al. (2020) and Liu et al. (2022) studied the impact of dust on convective clouds and the aerosol-cloud interactions in the Tibetan Plateau area. Mamun et al. (2021) used WRF-Chem to analyze the radiative and microphysical effects of Saharan dust over the East Atlantic Ocean. Chaibou et al. (2020) and Rizza et al. (2023) applied WRF-Chem model to quantify the effects of dust radiative forcing on West Africa and Mediterranean basin respectively and both suggested to include dust effects in climate studies to improve the accuracy of climate predictions.

In the present study, we will assess the role of aerosols through WRF-chem simulations of six case studies related to recent flooding events in the Liguria region, accompanied by significant Saharan dust plumes. The paper is organized as follows. Section 2 provides a short description of the considered events and of the WRF-Chem setting adopted to simulate the case studies. In Section 3, the different sets of performed simulations are analyzed and a discussion of the results is reported. Finally, conclusions are drawn in Section 4.

## 2. Material and methods

### 2.1. Event description

The present work will focus on the Liguria region (North-Western Italy), as it is one of the regions most affected by localized episodes of heavy rain in the Mediterranean (181 mm/h during 4 November 2011, 330 mm/3 h and 470 mm/6 h during 25 October 2011).

The peculiarity of this phenomenon is well known and widely described in a certain number of works (Rebora et al., 2013; Buzzi et al., 2014; Fiori et al., 2014; Cassola et al., 2016; Silvestro et al., 2016). Fig. 1 depicts the typical synoptic situation that is responsible for severe events over the region, showing the average mean sea level pressure [hPa] (panel a) and 500-hPa geopotential height [m] (panel b) observed during the most recent Liguria flooding events, listed in Table 1. Well visible is the low pressure west of the British Islands, facing the high pressure system affecting Eastern Europe. Such a configuration trigger two different flows: a cooler one, that from the Po valley reaches the Ligurian coast through low gaps present in the central part of Ligurian Apennines (blue arrow in Fig. 1, panel c), and a warm and moist southerly flow over Tyrrhenian Sea (red arrow in Fig. 1, panel c). The interaction between these two different flows causes the formation of a convergence line (yellow line in Fig. 1, panel c) which is often associated to the development of V-shaped, self-generating convective systems, responsible for heavy precipitation. In general, depending on the relative strength of the northerly and southerly fluxes, the convergence line and associated phenomena can affect different part of the region. If the eastward evolution of the low over western Europe is prevented by the eastern high pressure system, convergence line can remain stationary for several hours, resulting in devastating floods.

For the sake of brevity, here we only underline the extreme intensity and the small spatial extent of such events, as shown in Fig. 2, where the 12-h accumulated precipitation over the Liguria region is reported for the 6 events considered in the present work: 4 October 2010 (O10), 25 October 2011 (O11), 4 November 2011 (N11), 9 October 2014 (O14), 10 November 2014 (N14) and 21 October 2019 (O19). These events have been chosen inasmuch are the recentmost flooding events that affected the Liguria and present all ingredients we want to investigate in the present paper: a deep convective V-shaped system, consequence of the formation of convergence lines, accompanied by huge aerosol plumes due to strong southerly fluxes. The precipitation fields have been obtained by applying ordinary Kriging (Wackernagel, 1995) to point-wise observed data provided by the regional rain gauge network, Osservatorio Meteo Idrologico della Regione Liguria (OMIRL: https://omirl.regione.liguria.it, accessed on 16 May 2023), managed by the Ligurian Regional Environmental Protection Agency (ARPAL). The difference in spatial distribution of precipitation, and, in particular, the different localization of the precipitation peaks, is due to the different position of the convergence line between southerly and northerly flows that characterized all cases reported in Fig. 2. Indeed, although the large scale condition that triggered these events is roughly the same (Fig. 1), small differences in displacement of the western trough and/or eastern high, as well as local temperature gradient differences between Liguria inland and coast can affect the strength of the flows involved, resulting both in a different positioning of the convergence lines and in different intensity in precipitation (Cassola et al., 2016 and Buzzi et al., 2014).

### 2.2. AOD from MERRA-2 reanalysis

The synoptic configuration described in the previous paragraph and reported in Fig. 1 is also responsible for the generation and the transport of a considerable amount of Saharan dust towards the central Mediterranean basin (Rizza et al., 2017).

To characterize the total aerosol optical depth (AOD), we use the reanalysis from the Modern-Era Retrospective analysis for Research and Applications, Version 2 (MERRA-2 project; Gelaro et al., 2017). The aerosol data assimilation system in MERRA-2 is based on a splitting technique that is utilized to assimilate AOD at 0.55 μm from the following sources: (i) reflectance from the Advanced Very-High-Resolution Radiometer (AVHRR) sensor and from the MODIS on Terra (2000–present) and Aqua (2002–present) satellites; (ii) AOD retrievals
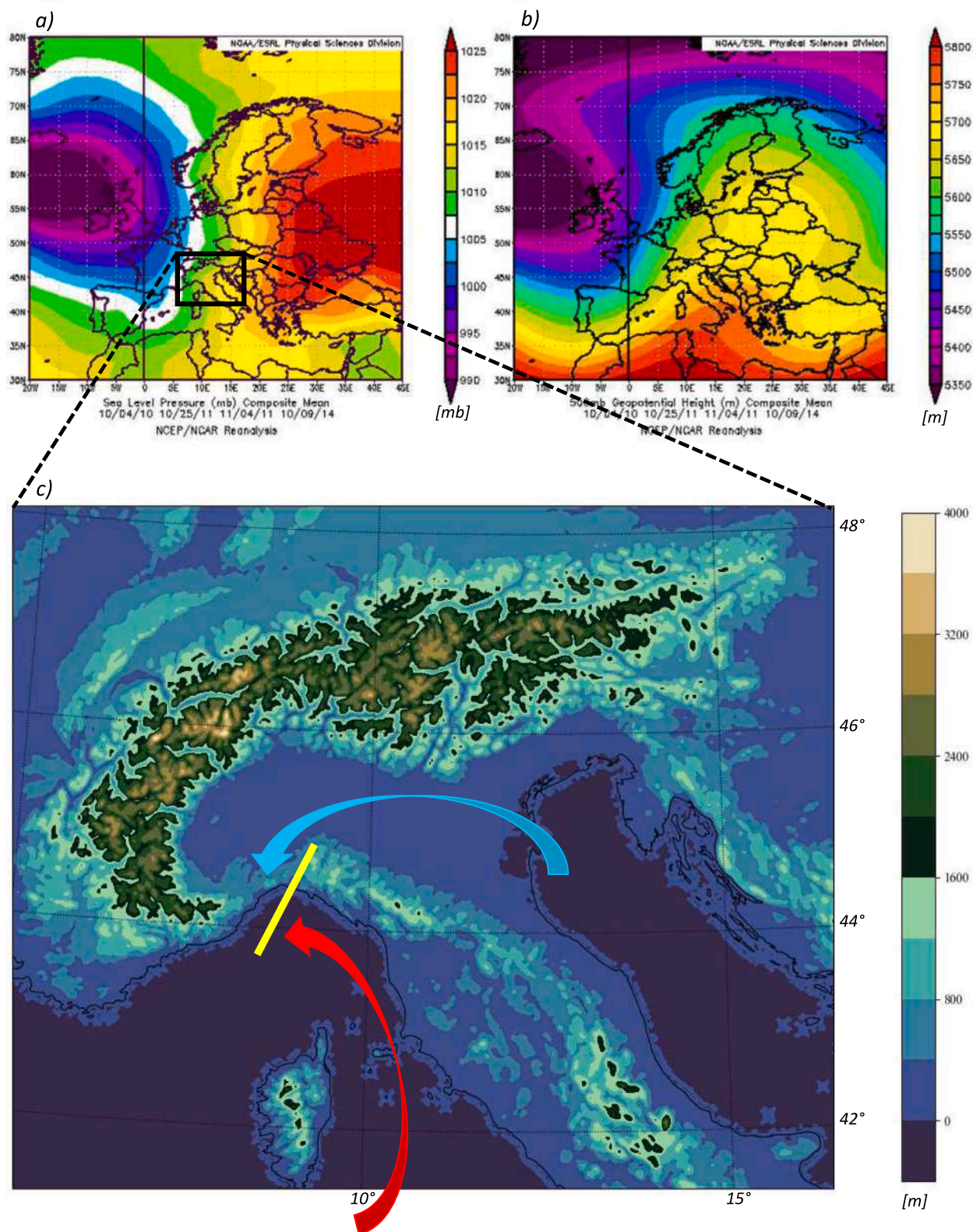
**Fig. 1.** Mean sea level pressure (hPa) (panel a) and 500-hPa geopotential height [m] (panel b) from NOAA-NCEP reanalysis, obtained by averaging the respective fields over 4 October 2010, 25 October 2011, 4 November 2011, 9 October 2014, 10 November 2014, and 21 October 2019. Source https://psl.noaa.gov/data/composites/day/, accessed on May, 162,023. Panel c: genesis of convergence line (yellow line) over Liguria region, as consequence of the interaction between a cold outflow coming from Po valley (blue arrow) and a warm and moist southerly flux over the Tyrrhenian Sea (red arrow). (For interpretation of the references to colour in this figure legend, the reader is referred to the web version of this article.)

**Table 1**

List and acronyms of the events analyzed in this study, and precipitation accumulated in 12 h.

| Event acronym | Event date | Precipitation max (mm) |
| --- | --- | --- |
| O10 | 04/10/2010 | 398 |
| O11 | 25/10/2011 | 493 |
| N11 | 04/11/2011 | 399 |
| O14 | 09/10/2014 | 268 |
| N14 | 10/11/2014 | 198 |
| O19 | 21/10/2019 | 479 |

from the Multiangle Imaging SpectroRadiometer (MISR); and (iii) AOD from AErosol RObotic NETwork (AERONET) measurements.

In Fig. 3, the total AOD, referred to the considered cases and obtained from MERRA-2 (Merra-2 'Global Modeling and Assimilation Office (GMAO)', *https://fluid.nccs.nasa.gov/reanalysis/chem2d_merra2/*, accessed on 10 May 2023), is shown.

The considered flooding events are accompanied by aerosol plumes

of different intensity and extension. These plumes are mainly composed of Saharan dust (Goudie and Middleton, 2001; Rizza et al., 2017), but during their travels over the Mediterranean Sea they are also enriched by sea spray aerosol particles generated at the sea surface under high wind speed conditions (Rizza et al., 2021).

The main objective of the present work is therefore to study what might be the role of aerosols in triggering and determining the evolution of Ligurian deep convective and flood events. This will be realized by activating the so-called direct aerosol-radiation interactions (Charlson et al., 1992; Kiehl and Briegleb, 1993; Rizza et al., 2023) and indirect aerosol-cloud interactions (Twomey, 1974; Twomey, 1991; Duan et al., 2019) in the WRF-Chem model.

Concerning the spatial distribution of aerosols characterizing the analyzed case studies, the effect of the presence of the incoming low pressure over western Europe (Fig. 1) is evident from Fig. 3. Such a synoptic configuration determined an intense transport of air masses from North Africa to Northern Italy that is highlighted by the band of aerosols affecting Northern Algeria, Sardinia and finally Northern Italy.
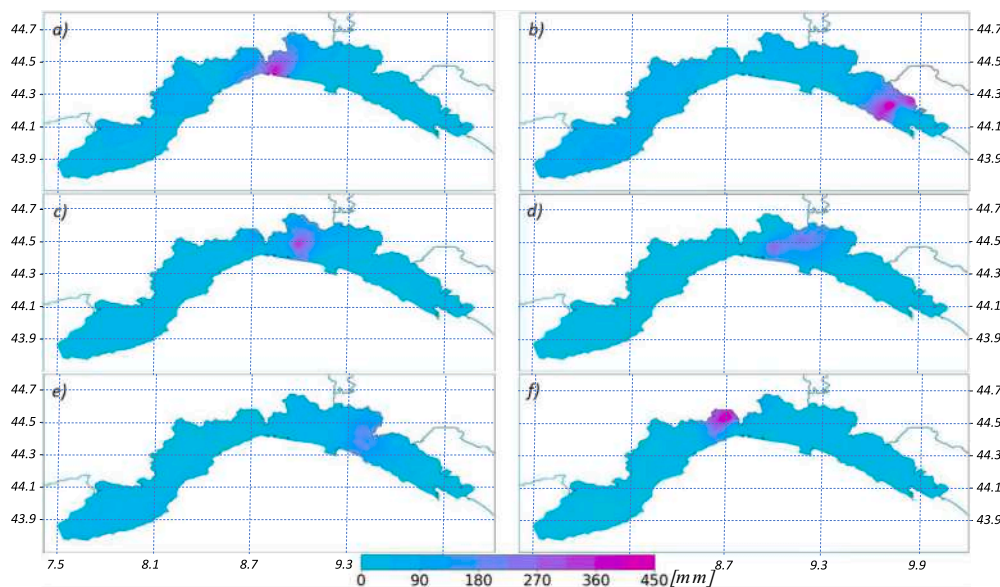


**Fig. 2.** 12-h accumulated precipitation (mm) during the six following events: a) O10, b) O11, c) N11, d) O14, e) N14, and f) O19.
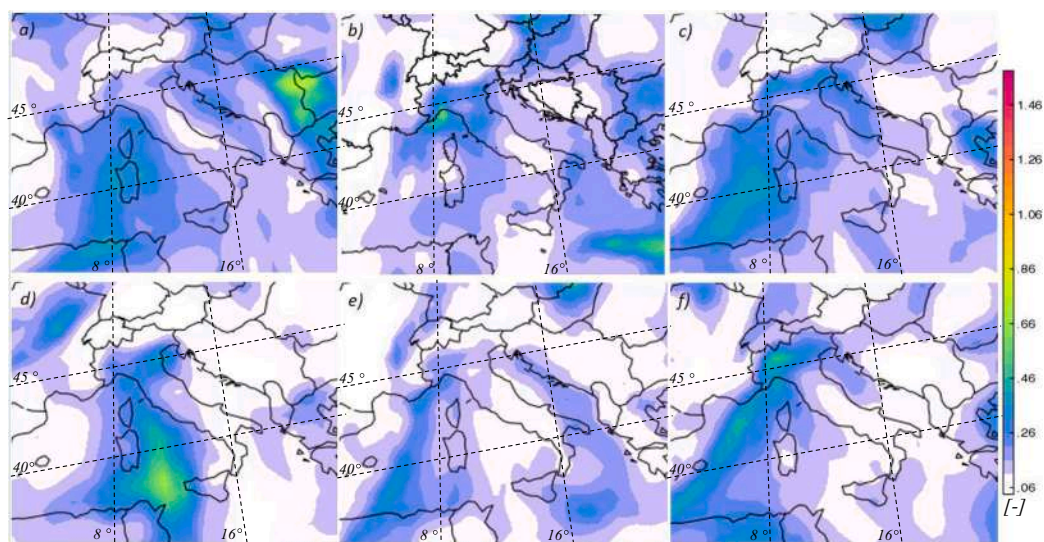


**Fig. 3.** Total Aerosol Optical Depth [−] for: a) 4 October 2010, 06 UTC, b) 25 October 2011, 09 UTC, c) 4 November 2011, 09 UTC, d) 9 October 2014, 12 UTC, e) 10 November 2014, 09 UTC and f) 21 October 2019, 09 UTC. Source MERRA-2, https://fluid.nccs.nasa.gov/reanalysis/, accessed on 10 May 2023.

Aerosol distribution patterns are quite similar for all cases; around the Liguria region and the Northern Tyrrhenian Sea, the values of the total AOD range between 0.3 and 0.7.

## 2.3. WRF-Chem setup

The present study is carried out through numerical simulations performed with the Weather Research and Forecasting coupled with chemistry (WRF-Chem) model, version 4.0 (Grell et al., 2005). WRF-Chem simulates the emission, transport, mixing, and chemical transformation of trace gasses and aerosols as well as the meteorology. In this work we performed three different sets of simulations (Table 2). First, a control run (referred to as ctrl_run), in which the chemistry package of WRF-Chem model has not been activated (corresponding to the option *chem_opt = 0* in the WRF namelist), i.e., a WRF standalone run. Then, a second run in which the chemistry package is turned on but only aerosol indirect effects are considered (MP_fdb). Namely, aerosol is enabled to act as Cloud Condensation Nuclei (CCN) and Ice Nuclei (IN) (Levin and Cotton, 2009; Tao et al., 2012). Finally, a fully-coupled (fully_cpl) run in which both direct and indirect effects are taken into account (Fast et al., 2006).

For a correct representation of the events listed in Table 1, characterized by the formation of small-scale very deep convective systems, we need to reach a resolution allowing an explicit description of convection as highlighted by a number of previous works in the Mediterranean region (Miglietta and Regano, 2008; Fiori et al., 2014; Cassola et al., 2015; Davolio et al., 2015; Gascon et al., 2016). For this purpose, we defined three 2-way nested domains that are displayed in Fig. 4 and described in Table 3. The innermost domain, centered over the Liguria Region, will allow us to analyze models' data at 1.1 km grid spacing with convection explicitly resolved. The limited number of vertical levels is constrained by the considerable computational effort required for the treatment of the aerosols.

Regarding the WRF model settings to describe the effects that unresolved sub-grid phenomena have on resolved variables, we have chosen a physical set-up that is quite similar to those exploited for similar studies (Cassola et al., 2015; Ferrari et al., 2020), briefly recalled in the following and summarized in Table 4.

The Yonsei University Planetary Boundary Layer (YSU-PBL) scheme (Hong et al., 2006) was selected together with the Revised MM5 Monin-Obukhov scheme (Jimenez et al., 2012) for the surface layer parameterization and Noah scheme for land surface model (Chen and Dudhia, 2001). Convection being explicitly resolved over the two innermost domains, Grell-Freitas cumulus parameterization scheme (Grell and Freitas, 2014) was adopted only for the outermost domain. For short-wave and longwave radiation schemes we adopted the Rapid Radiative Transfer Model for General Circulation Models (RRTMG) (Clough et al., 2005; Iacono et al., 2008) to consider the cloud and aerosol effects in the radiative flux calculation.

Finally, motivated by the necessity to couple the meteorological part of the WRF-ARW model with its chemical part, for the Microphysics scheme we chose the Morrison parameterization (Morrison et al., 2009). It is a double-moment bulk scheme predicting the mass mixing ratios and number concentrations of five hydrometeor species: cloud droplets, cloud ice, snow, rain, and graupel. The double-moment Microphysics scheme indeed can interact with the aerosol modules, allowing (in the case of simulations MP_fdb and fully_cpl) to couple the activation of

**Table 2**
Summary of the three different settings exploited for simulations performed in the present work.

| Acronym | Microphysics feedback | Radiative feedback |
|---|---|---|
| ctrl_run | no | no |
| MP_fdb | yes | no |
| fully_cpl | yes | yes |

aerosol particles to the scheme itself (Morrison et al., 2009). In two-moment bulk schemes, hydrometeor size distributions are diagnosed from the predicted number and mass assuming a certain distribution of the spectral shape (in most cases a gamma function). Usually, in these schemes, the saturation adjustment approach is used for calculating evaporation and condensation, i.e. under-saturation and supersaturation with respect to water are removed in the cloud within a time step (Zhang et al., 2015).

The physical parameterizations, described in Table 4, are kept fixed for all simulations. The differences between the three configurations depend on the radiation feedback. In the runs MP_fdb the radiation feedback is not activated and only the interaction between aerosol and clouds has been enabled, i.e. aerosols acted as CCN and IN, but aerosol direct radiative forcing has been neglected. For simulations fully_cpl, instead, the radiation feedback is enabled in order to take into account also the forcing deriving from the interaction between radiation and aerosol.

For both simulations MP_fdb and fully_cpl, we adopted the Model for Ozone and Related chemical Tracers (MOZART) Chemistry (Emmons et al., 2009) coupled with the four-size bin sectional Model for Simulating Aerosol Interactions and Chemistry (MOSAIC) aerosol mechanism (Zaveri et al., 2008). MOZART-MOSAIC takes into account several interactions between different chemical species present in the aerosol, including aqueous phase chemistry, plus photolysis and wet and dry deposition (Baró et al., 2015; Knote et al., 2015).

To provide WRF-Chem with a reliable initial aerosol field, MERRA-2 (Gelaro et al., 2017) data were ingested into the model through the Merra2BC preprocessor (Ukhov et al., 2021), that is an interpolation utility for boundary and initial conditions. The utility, originally prepared to work with eight-size aerosol sectional bins, has been modified to remap the MERRA-2 data into the four aerosol sectional bins adopted by the MOZART-MOSAIC package (dry diameters of 0.039–0.156 μm, panel a, 0.156–0.625 μm, panel b, 0.625–2.500 μm, panel c and 2.5–10.0 μm, panel d).

For each event, three 48-h simulations have been carried out according to the three different configurations described above (6 events for the 3 different settings of WRF-Chem). All simulations have been initialized at 00 UTC of the day of the event itself starting from atmospheric initial conditions provided by Global Forecast System (GFS) global model and from aerosol initial fields provided by MERRA-2. Boundary conditions, relative to both the atmospheric and aerosol fields, have been provided to the WRF-Chem model every three hours. As the aerosol distribution is calculated in a way consistent with MERRA-2 meteorological fields, the consistency between the meteorological fields provided in MERRA-2 and GFS has been preliminary verified.

## 3. Results and discussion

### 3.1. Aerosol optical depth

The first step of the present analysis is a qualitative 'eyeball' verification of the ability of the model to reproduce the evolution of the Saharan dust during the analyzed case studies. In Fig. 5, the AOD simulated by the WRF-Chem fully-coupled runs over the outermost domain, for all case studies, is reported.

By comparison with Fig. 3, one can appreciate how the order of magnitude of AOD and its spatial distribution are well reproduced over the central Mediterranean basin. Simulations capture the aerosol plume west of the Italian peninsula that was observed during all considered cases. The six snapshots of Fig. 5 reveal strong intrusions of Saharan dust in all six cases that we are analyzing.

### 3.2. Analysis of winds

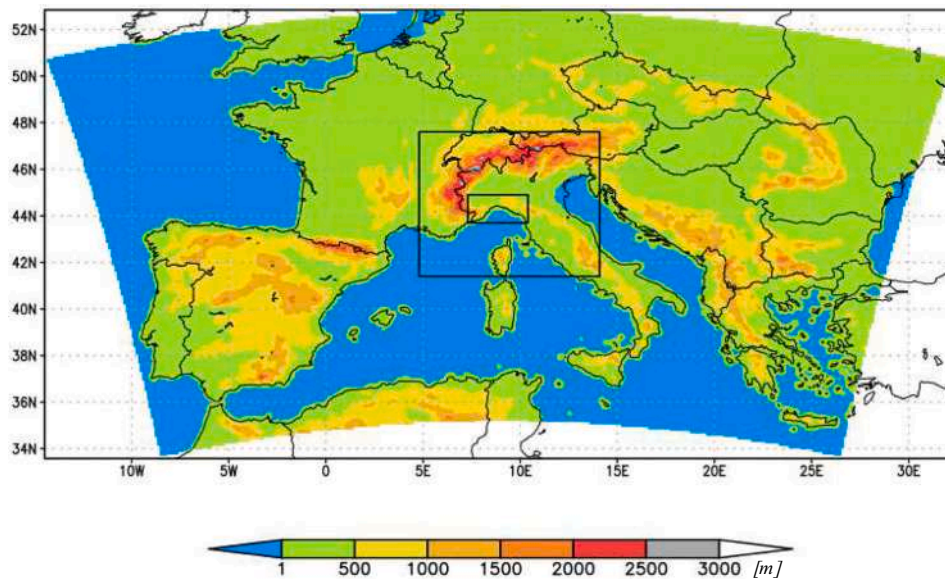Keeping in mind that winds are the main trigger of the analyzed V-

**Fig. 4.** Topography (m) of the outermost WRF computational domain (10 km grid spacing) and location of the two nested domains over northern Italy (outermost box, 3.3 km grid spacing) and Liguria region (innermost box, 1.1 km grid spacing).

**Table 3**
Relevant features of the computational domains: horizontal grids spacing and number of vertical levels.

| Domain | (dx,dy) km | nz |
| --- | --- | --- |
| Outermost | 10,10 | 35 |
| Intermediate | 3.3,3.3 | 35 |
| Innermost | 1.1,1.1 | 35 |

**Table 4**
Overview of the WRF parameterization schemes adopted in the present study.

| Parameterization scheme | Physical process | Namelist option | References |
| --- | --- | --- | --- |
| Grell-Freitas | Convection | 3 | Grell and Freitas, 2014 |
| Morrison | Microphysics | 10 | Morrison et al., 2009 |
| Rapid Radiation Transfer Model GCM | Long wave radiation | 4 | Clough et al., 2005 |
| Rapid Radiation Transfer Model GCM | Short wave radiation | 4 | Clough et al., 2005 |
| Noah | Land surface | 2 | Chen and Dudhia, 2001 |
| Monin-Obukhov | Surface layer | 1 | Jimenez et al., 2012 |
| Yonsei University | Boundary layer | 1 | Hong et al., 2006 |

shaped convective systems, we passed to analyze the effect of aerosol on the simulated weather conditions. The first significant result concerns the important attenuation of the wind intensity in all fully-coupled simulations (runs fully_cpl) with respect to the control runs (ctrl_run). Attenuation appears to affect both southerly and northerly flows associated to the convergence line formation. In previous works, a similar attenuation was also observed and has been mainly related to the reduction of downward shortwave flux at the ground due to aerosol interception, that, in turn, decreases the near-surface energy (Zhang et al., 2015; Rizza et al., 2023).

Our finding is further corroborated by direct comparison of the wind fields from ctrl_run and MP_fdb, which turn out to be very similar, thus confirming the role of the aerosol-radiation feedback. Focusing on the wind field, the added value of running a coupled atmospheric-chemistry

simulation appears to reside in the aerosol-radiation feedback rather than in the cloud-aerosol interaction. For the sake of brevity, just an example of a wind field simulated by the three different WRF settings is reported in Fig. 6. The latter refers to the 25 October 2011 case study inasmuch it is one of the most interesting events in terms of precipitation, and for this reason will be analyzed in depth in the following section.

From the analysis of Fig. 6 it emerges how ctrl_run (Fig. 6a) and MP_fdb (Fig. 6b) present a similar wind field when compared with the simulation fully_cpl (Fig. 6c). Similarities in the simulated wind fields concern both wind intensity and the position of the convergence line. Indeed, both simulations ctrl_run and MP_fdb localize the convergence line exactly in the same position, while the simulation fully_cpl shifts it about 30 km eastward. For the sake of brevity, wind fields referring to other events are not reported in the text; in Table 5 the average wind intensity for all events is reported instead. In more detail, the values summarized in the table refer to a spatio-temporal average over the 12 h covering the events and over the two areas indicated by the two squared boxes in Fig. 6a. The two boxes are located in correspondence of areas typically affected by northerly (N) and southerly flows (S) that give rise to the convergence line responsible for the extreme events studied in the present work. The values reported in Table 5 display a general decrease of the wind speed in the simulations fully_cpl compared to the wind speed from ctrl_run. This reduction seems to affect both northerly and southerly flows, even if more importantly the first one, a fact which concurs to significantly attenuate the strength of the convergence line.

To explain the wind attenuation associated with simulations fully_cpl, in Fig. 7a the AOD, averaged between 00 UTC and 12 UTC of 25 October 2011, is reported as provided by the simulation fully_cpl. Fig. 7b shows the difference between the mean surface downward longwave radiation from simulations fully_cpl and from ctrl_run. The resulting difference is averaged in the same time span of panel a).

Although the focus here is on the 25 October 2011 event, the conclusions we are going to draw hold true for the other analyzed events too (not shown).

The aerosol layer absorbs part of the longwave radiation emitted by the surface causing, in turn, an increase in the longwave radiation emitted by the lower atmosphere towards the surface. Because of the absorption and the associated re-emission of atmospheric radiation by aerosol species, the higher the aerosol concentration, the higher the longwave flux observed at the surface (Satheesh and Lubin, 2003;
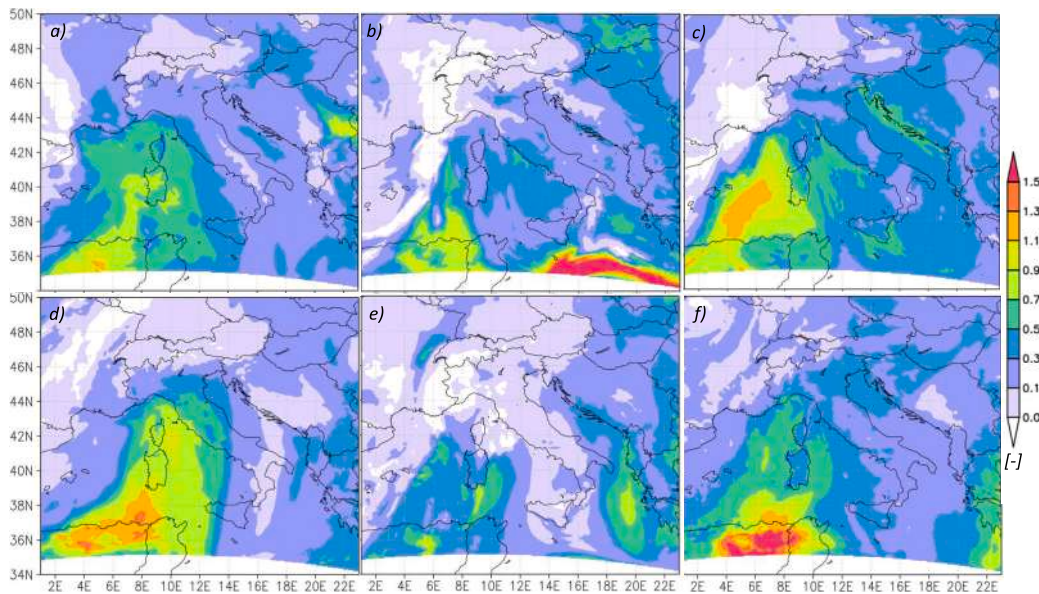
**Fig. 5.** Aerosol Optical Depth for: panel a), 4 October 2010, 06 UTC, b), 25 October 2011, 09 UTC, c), 4 November 2011, 09 UTC, d), 9 October 2014, 12 UTC, e), 10 November 2014, 09 UTC and f) 21 October 2019, 09 UTC, from simulation fully_cpl over the outermost domain.

Panicker et al., 2008). The increase of downward longwave radiation in the simulation fully_cpl with respect to ctrl_run (Fig. 7, panel b) is indeed stronger where values of AOD are higher (Fig. 7, panel a), reaching maximum values of the order of 30%.

Due to the different specific heat between land and sea, the increased flux of downward longwave radiation heats up in different ways the Mediterranean Sea and the surrounding lands (Fig. 7, panel d). Keeping in mind that the considered events occurred in the first part of autumn, when the sea surface temperature is usually warmer than land temperature, as shown in Fig. 7, panel c, the overall effect of the increased downward longwave radiation flux simulated by the run fully_cpl is to reduce the ctrl_run land-sea temperature gradient. Hence, the simulation fully-coupled produced a more homogeneous surface temperature distribution with respect to the simulation ctrl_run, finally resulting in a wind speed reduction. A similar mechanism is described, for example, in (Park and van den Heever, 2022), where, in case of polluted air, a smaller land–sea thermal contrast and a resulting weaker sea breeze circulation is observed with respect to the pristine case.

In our cases, the effect played by the downward shortwave radiation is less relevant with respect to what is found in other works (see, e.g., Rizza et al., 2023). This can be explained as a consequence of our focus on short time windows (about 12 h), during which the relevant cloud cover that characterized the studied events reduced the amount of shortwave radiation that reached the lowest atmospheric layer and the surface. This fact made secondary the effect of interaction between shortwave radiation and aerosol with respect to the role of longwave radiation. When analyses are instead based on a longer time period with respect to the typical lifespan of a convective system, the overall cloud effect is reduced and the interaction between shortwave radiation and aerosol becomes relevant.

*3.3. Analysis and discussion of precipitations patterns*

The overall wind attenuation associated with the simulation fully_cpl resulted in a significant attenuation of the convergence line as shown in Fig. 8 referring to 15 UTC of 25 October 2011. Here the 10-m wind field divergence is reported for simulations ctrl_run, panel a), MP_fdb, panel b), and fully_cpl, panel c).

As a consequence of the attenuation of the convergence lines simulated by the runs fully_cpl, one would expect an attenuation of the precipitation as observed in numerous previous works (Cassola et al.,

2016; Ferrari et al., 2021), since the weaker the convergence, the weaker the associated upward motions, arguably resulting in reduced convection and precipitations. On the contrary, for half of the analyzed cases (4 October 2010, 25 October 2011 and 4 November 2011), simulations fully_cpl show a precipitation maximum increase between 15% and 35% with respect to the ctrl_run.

At the same time, for the remaining cases (9 October 2014, 10 November 2014 and 21 October 2019) a less surprising decrease of precipitation maximum, of the order of 10% - 30%, is observed as a consequence of the weakening of the convergence line simulated by runs fully_cpl.

In the following, we will focus on those events whose simulations showed, unexpectedly, an intensification of the precipitation in spite of the reduced convergence. In Figs. 9, 12 hours accumulated precipitation during the 25 October 2011 event for ctrl_run, panel a), MP_fdb, panel b), and fully_cpl, panel c), is shown.

The increase of the precipitation simulated by runs fully_cpl, evident in Fig. 9 and also evident from simulations of 4 October 2010 and 4 November 2011 events (not shown), is indeed somehow independent of the intensity of the convergence lines, that appear weaker in the simulations fully_cpl with respect to both runs ctrl_run and MP_fdb. Apparently, the precipitation increase is not a consequence of the sole aerosol-cloud interaction, inasmuch simulations MP_fdb and ctrl_run present quite similar scenarios both in relation to the resulting wind field and precipitation patterns, and intensity.

Ultimately, the fully coupled cloud-aerosol-radiation interaction appears to play a fundamental role in the description of this subset of events. To further highlight the impact of the three different model setting on precipitation field, in Fig. 10 the 12-h accumulated precipitation difference between simulations fully_cpl and ctrl_run, panel a), and between fully_cpl and MP_fdb, panel b), is shown. Well evident is the eastward displacement of the precipitation peak associated to simulation fully_cpl due to the shift of the convergence line observed in Fig. 8. Trying to explain the mechanisms at the basis of the results obtained by the different sets of simulations, in Fig. 11, panel *b*) the vertical cross section of the aerosol fraction referred to as other inorganic mass (OIN) [μg kg$^{-1}$-dry air], is reported. OIN particles that contain the crustal and dust particles, are mainly composed by inert minerals, trace metals and sea salt (Zaveri et al., 2008). The vertical cross section refers to 15 UTC of 25 October 2011 and is taken at 44° N, in correspondence with the red line present in Fig. 11, panel *a*), showing the corresponding 10 m wind
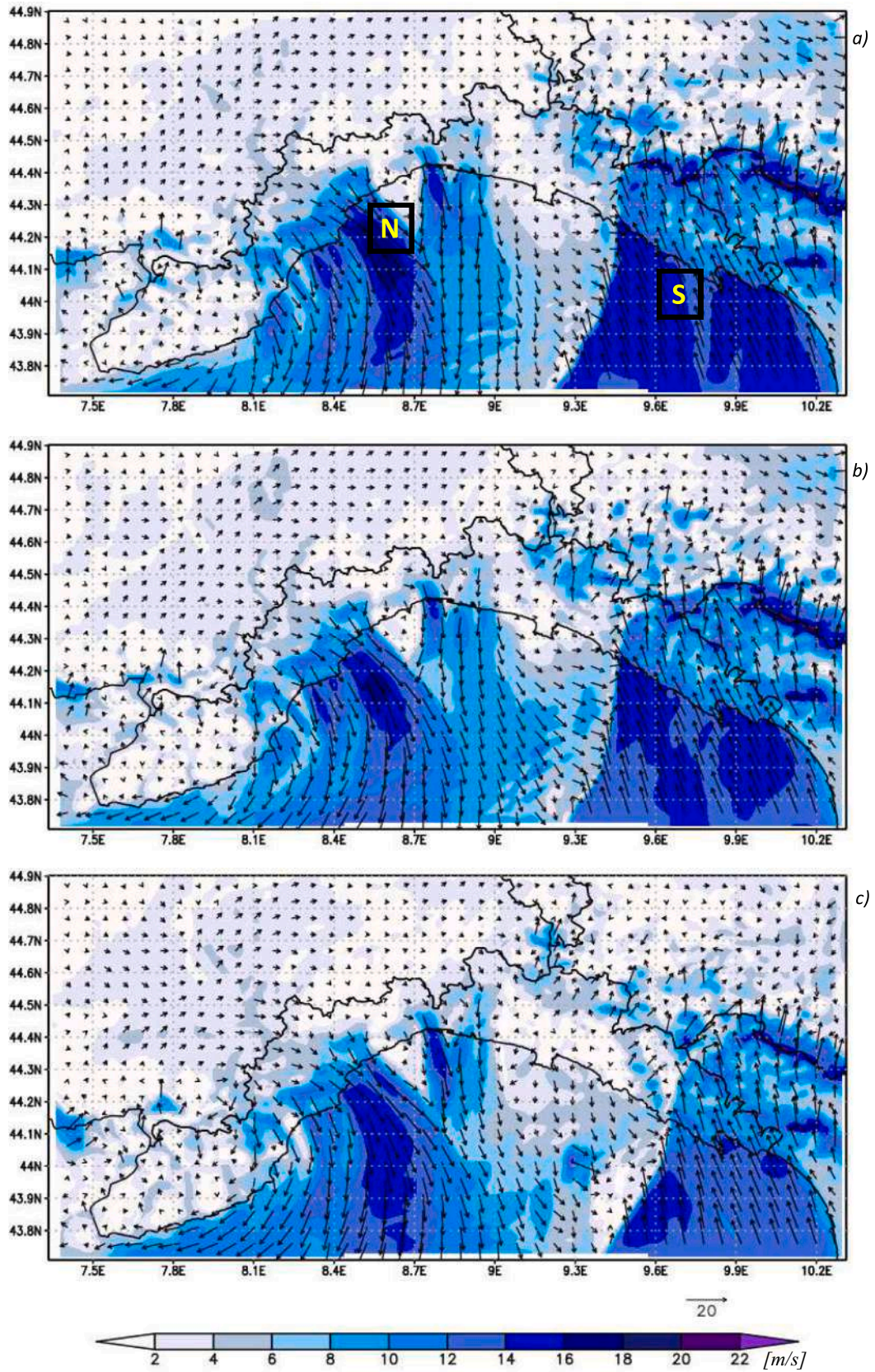
**Fig. 6.** 10 m wind field (m s$^{-1}$) referred to 25 October 2011, 15 UTC, simulated over 1.1 km domain by: ctrl_run, panel a), MP_fdb, panel b), and fully_cpl, panel c). In panel a) the location of the two squared boxes (N, S) is reported.

**Table 5**

Spatio-temporal average of 10 m wind speed [m s$^{-1}$], for all considered events, and for simulations ctrl_run, MP_fdb and fully_cpl. Columns N and S indicate that the spatial average of the wind speed has been performed over the two boxes reported in Fig. 6, panel a). Winds have also been averaged over a 12-h window centered around the precipitation peak of each event.

| Event | Spatio–temporal average of 10 m wind intensity (m s$^{-1}$) | | | | | |
|---|---|---|---|---|---|---|
| | ctrl_run | | MP_fdb | | fully_cpl | |
| | N | S | N | S | N | S |
| 4 Oct 2010 | 11.1 | 12.7 | 11.1 | 12.8 | 10.4 | 12.7 |
| 25 Oct 2011 | 12.8 | 12.8 | 12.9 | 12.1 | 12.5 | 10.5 |
| 4 Nov 2011 | 9.2 | 12.2 | 9.4 | 12.3 | 9.4 | 12.3 |
| 9 Oct 2014 | 8.4 | 8.6 | 8.3 | 8.4 | 5.8 | 8.1 |
| 10 Nov 2014 | 7.1 | 8.4 | 6.7 | 9.0 | 5.4 | 8.7 |
| 21 Oct 2019 | 2.9 | 6.3 | 2.9 | 6.3 | 2.4 | 4.7 |

field. The position of the vertical cross section has been chosen over the sea, south of the precipitation peak, in order to evaluate the characteristics of the flows that originate the convergence line, filtering out the disturbances on the low level flows induced by the local steep orography. The largest concentration of aerosol is associated with the southerly flow, and presents its maxima in the lower layers, at about 900 hPa.

A further smaller concentration peak is visible in correspondence of 8.7°E, associated to the northerly flow and probably due to the outflow of continental anthropogenic pollutants. This fact seems to be confirmed by Fig. 12, showing the cross section of the OIN concentration (contours, [µg kg$^{-1}$-dry air]) for the four-size bins taken into account by MOSAIC, taken at 44°N and at 15 UTC of 25 October 2011. According to (Juda-Rezler et al., 2020), finer aerosol particles, namely with aerodynamic diameter smaller than 2.5 µm, are mainly associated with anthropogenic emission, while dust aerosol is typically characterized by larger aerodynamic diameters, usually between 0.6 µm and 10 µm (Marenco et al., 2006).

From Fig. 12 it emerges how, by increasing the dry diameters of the

aerosol, their concentration maxima move from west to east, i.e., from the area affected by the low-level northerly flow to the area affected by the southerly flow (Fig. 6, panel c)). Focusing on the thermal effect that this aerosol distribution produces in the simulations, in Fig. 13, the vertical cross section of temperature difference (K) between fully_cpl and ctrl_run is also reported (shaded contours).

Once again, the added value associated with running a chemistry-atmosphere coupled simulation appears to reside in the aerosol direct radiative forcing. Comparing the vertical cross section of temperature difference (K) between simulations fully_cpl and ctrl_run reported in Fig. 12 with the vertical cross section of temperature difference (K) between simulations MP_fdb and ctrl_run of Fig. 12, panel b), it emerges how the temperature difference between MP_fdb and ctrl_run results significantly attenuated with respect to the temperature difference between simulations fully_cpl and ctrl_run.

Similar vertical dust patterns are also found for simulation fully_cpl for 4 October 2010 and 4 November 2011 (not shown).

Trying to explain the significant precipitation increase simulated by run fully_cpl with respect to simulations ctrl_run and MP_fdb, in Fig. 14, the vertical cross section (same time and latitude of Fig. 13) of the water vapor mixing ratio (shaded contours, [kg kg$^{-1}$]) is reported together with the OIN concentration (contours, [µg kg$^{-1}$-dry air]). The largest concentration of water vapor is found east of the convergence line (black star in Fig. 14) and occupies the same levels of the OIN. The warming of these moist layers by the interaction between aerosol and radiation increased the instability as shown in Fig. 15. Here, the simulated soundings extracted just east of the convergence line at 44.15°N and 9.6°E for fully_cpl, panel a), MP_fdb, panel b) and ctrl_run, panel c), are reported. In particular, soundings refer to 09 UTC, just some hours before the beginning of the event. Panel c) shows a more saturated layer between 850 hPa and 600 hPa with respect to simulations ctrl_run and MP_fdb, respectively panels a) and b). For all three soundings, the Convective Available Potential Energy significantly varies, passing from 160 J kg$^{-1}$ for ctrl_run, to 271 J kg$^{-1}$ for MP_fdb, and reaching 441 J kg$^{-1}$ for simulation fully_cpl. The higher instability and the larger lower
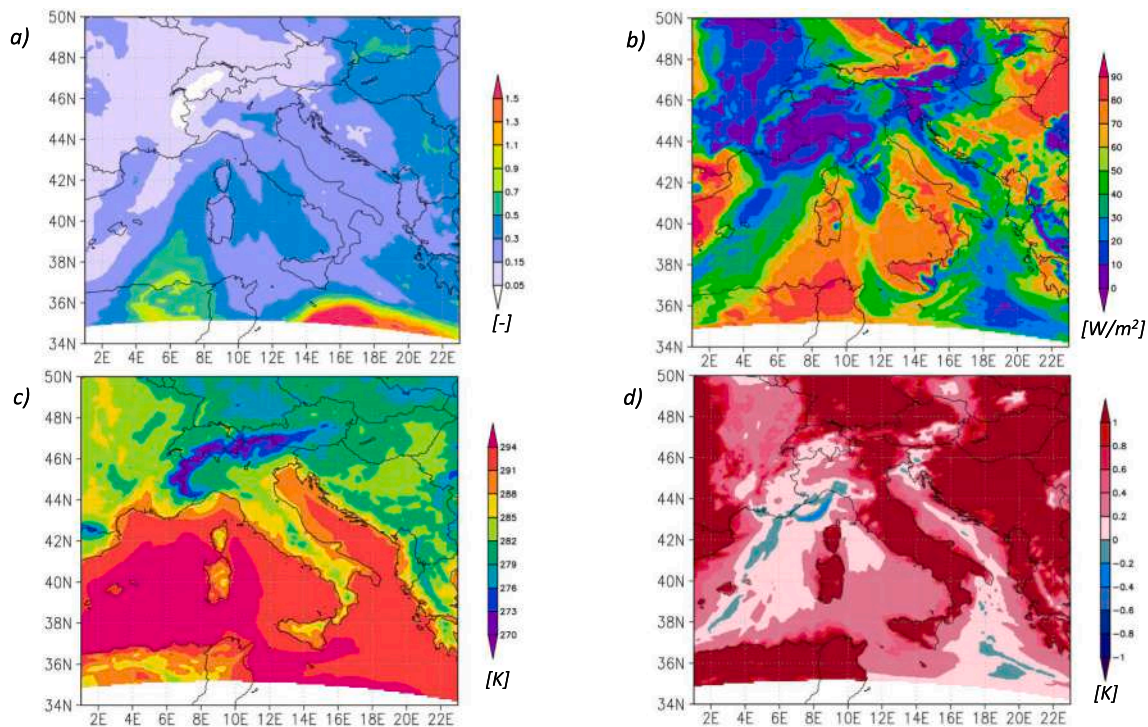


**Fig. 7.** Panel a): AOD provided by simulation fully_cpl. Panel b): surface downward longwave radiation difference between simulations fully_cpl and ctrl_run. Panel c): 2 m temperature (in K) provided by ctrl_run. Panel d): 2 m temperature difference between simulations fully_cpl and ctrl_run. All plotted quantities are provided by 10 km grid spacing simulations and averaged between 00 and 12 UTC of 25 October 2011.
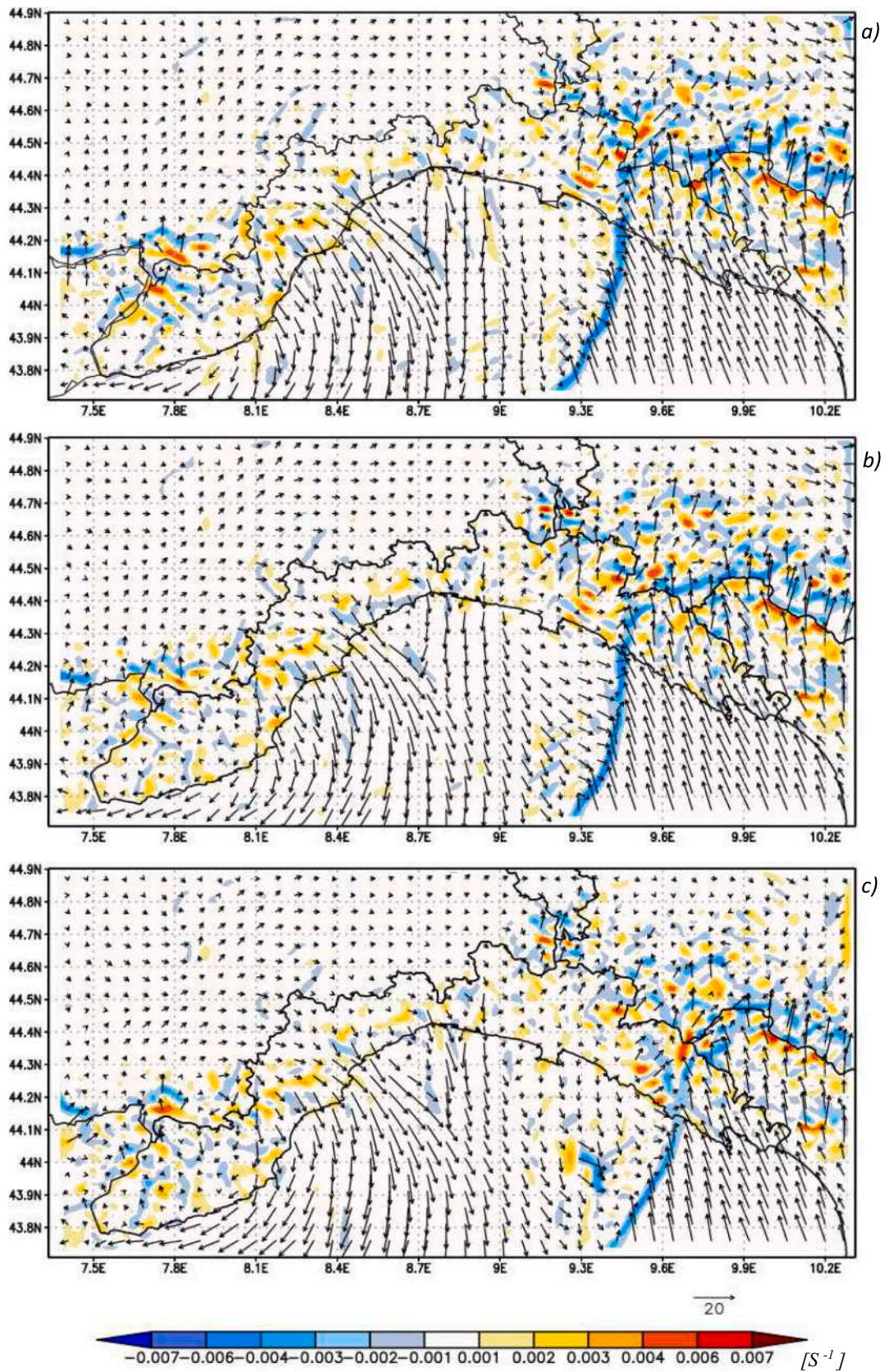
**Fig. 8.** 10 m wind (vectors, m s$^{-1}$) and divergence (shaded contours, s$^{-1}$) fields for simulations ctrl_run, panel a), MP_fdb, panel b), and fully_cpl, panel c), simulations referring to 15 UTC of 25 October 2011.
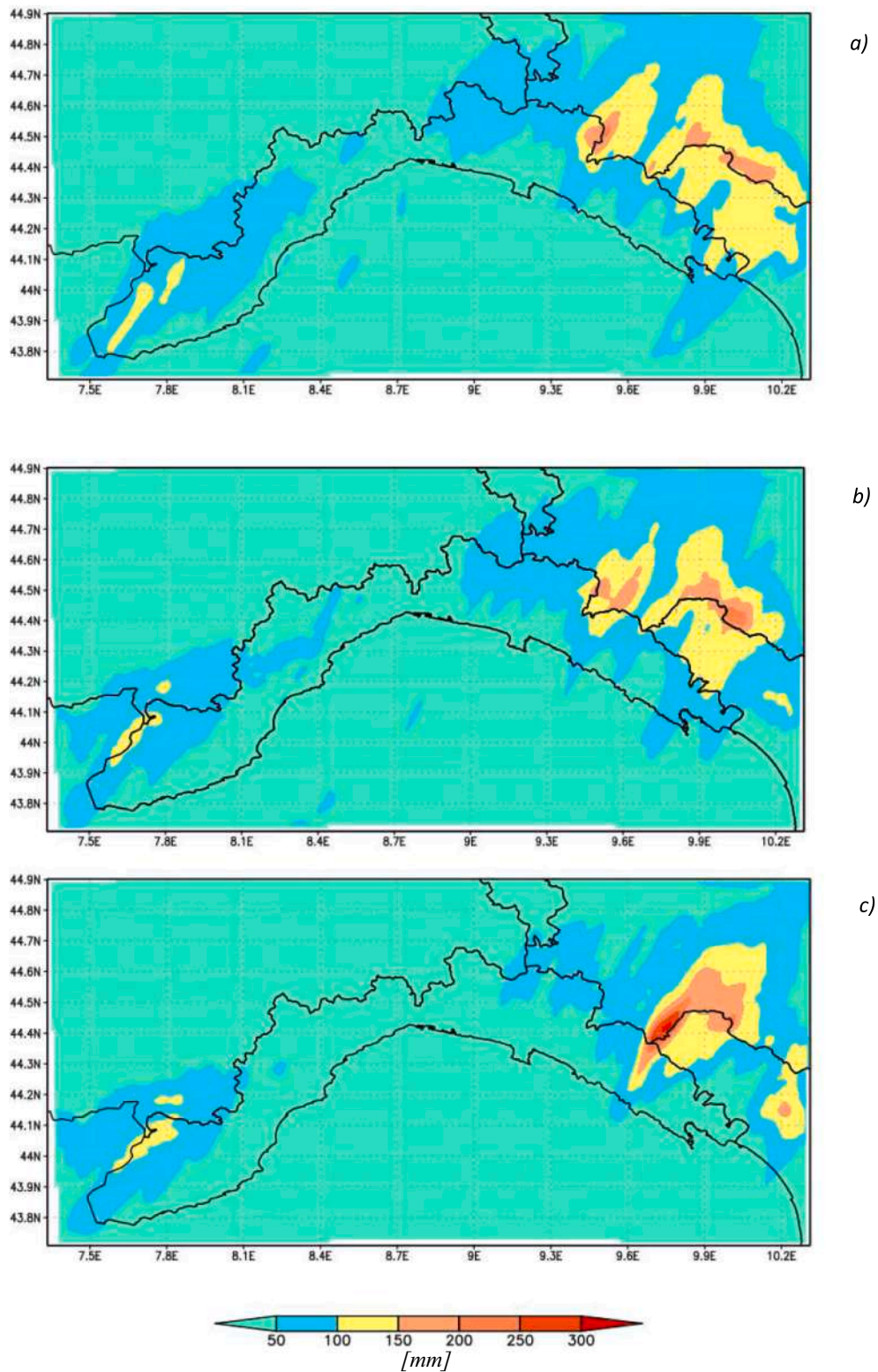
**Fig. 9.** 12-h accumulated precipitation (unit: mm) for the 25 October 2011 event, provided over 1.1 km domain by simulations: ctrl_run, panel a), MP_fdb, panel b) and fully_cpl, panel c).

layers humidity content found in simulation fully_cpl with respect to ctrl_run one is able to trigger a deeper convective cell responsible for the flood. The development of this convective cell is identifiable by the increment of temperature at about 500 hPa visible in Fig. 13, associated with the release of latent heat due to water vapor condensation in the convective cloud.

## 4. Conclusions

In the present work, we have investigated the influence played by the so-called direct (aerosol-radiation) and indirect (aerosol-cloud) interactions on the dynamics of mesoscale V-shaped convective systems. Three different sets of simulations have been carried out with the WRF-
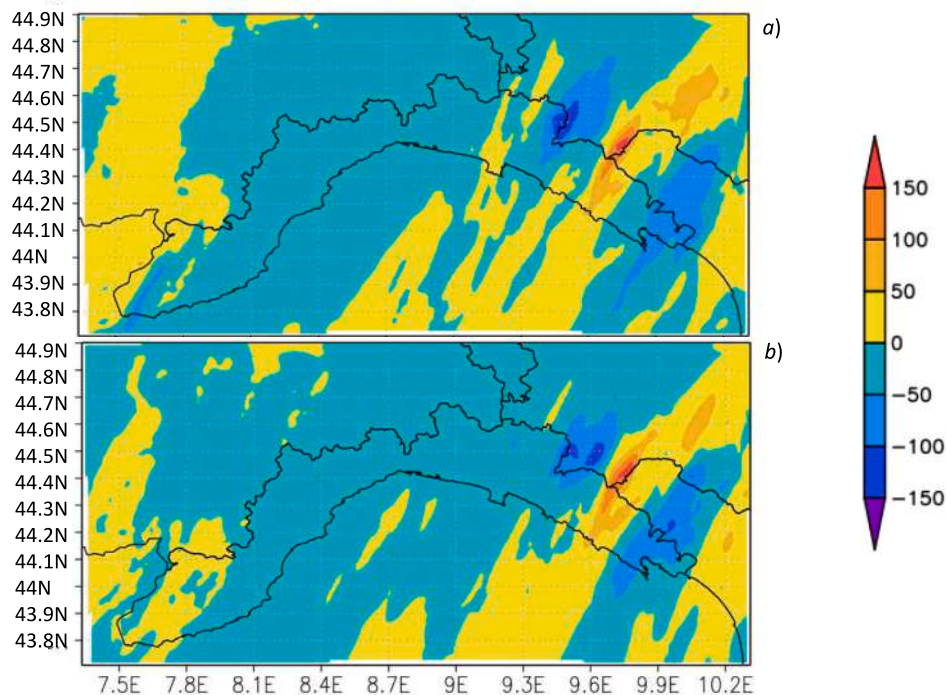
**Fig. 10.** 25 October 2011, 12-h accumulated precipitation difference (unit: mm) between simulations: fully_cpl and ctrl_run, panel a), fully_cpl and MP_fdb, panel b).

Chem model, namely control runs (ctrl_run) without chemical coupling, runs taking into account only the aerosol indirect effects (MP_fdb) and fully coupled simulations taking into account both direct and indirect effects (fully_cpl).

Six different events concerning recent floods that occurred in the Liguria region have been simulated according to the three different WRF-Chem settings. All these events are characterized by the formation of convergence lines, associated to quasi-stationary, V-shaped, self-generating convective systems over the Ligurian Sea due to the interaction between two different low-level flows. The two main features concurring in the determination of the intensity, localization and evolution of these systems are the strength of the convergence lines, that is able to trigger vertical motions, and the conditional instability of the lower layers that can enhance or dampen the triggered ascending motions. A correct description of these two factors is indeed essential to provide a reliable evolution of the flooding events.

The most relevant finding is on the direct effects associated with the aerosol-radiation feedback that appears to overcome the aerosol indirect effect. This second one does not seem to produce relevant impacts on the simulations of the considered events: wind, temperature and precipitation fields produced by simulations MP_fdb are indeed very close to those produced by the corresponding ctrl_run. On the other hand, direct effects have stronger impact on simulations, causing a significant attenuation of surface winds, and hence of the convergence lines, in all performed simulations. This attenuation has been traced back to the interaction between shortwave radiation and aerosol that causes a reduction of the sea-land thermal gradient, finally resulting in a weakening of the wind.

Because of the absorption and associated re-emission of atmospheric radiation by aerosol species, the increase of downward longwave radiation observed in the runs fully_cpl with respect to simulations ctrl_run is stronger where the values of AOD are higher (Satheesh and Lubin, 2003; Panicker et al., 2008). As long as the studied events happened in the first part of Autumn, when the sea surface temperature is warmer than land temperature, the increased surface downward longwave radiation reduces the temperature gap between land and sea owing to the different specific heat between land and water.

Hence, the simulations fully_cpl produced a more homogeneous surface temperature distribution with respect to the simulations ctrl_run that results in an attenuation of the winds, i.e. the contribution of the local circulation is strongly attenuated. This mechanism is coherent with what has been found in other works, for example, in Park and van den Heever (2022) where, in case of polluted air, a smaller land–sea thermal contrast and a weaker sea breeze circulation is observed with respect to the pristine case.

In our work, the effect of downward shortwave radiation appears to be less relevant with respect to what has been found in other studies (e. g., Rizza et al., 2023). Our analysis focused on time windows of about 12 h, during which the relevant cloud cover that characterized the studied events reduced the amount of shortwave radiation that reached the lowest atmospheric layer and the surface. When analyses are instead based on a longer time period with respect to the typical lifespan of a convective system, the overall cloud effect is reduced and the interaction between shortwave radiation and aerosol becomes relevant.

With regard to convection associated to the studied events, convergence is certainly the main dynamical forcing triggering V-shaped convective systems in the considered area, as highlighted by numerous works. Miglietta and Davolio (2022) reported that the convergences that affect Liguria Sea and responsible for the formation of V-shaped systems, produce an uplift of the low-level moist air, sufficient to overcome the level of free convection and thus allow the release of convective energy. Furthermore, this kinematic interaction was suggested and somehow observed through airborne and ground-based radar observations already during the Mesoscale Alpine Programme field campaign in 1999 (Bougeault et al., 2001). Also, Cassola et al. (2016) showed that a stronger convergence enhances convective development. In our work however, the weaker convergence lines simulated by the simulations fully_cpl are not always associated, as one would expect, to a weaker and shallow convection resulting in a decrease in precipitation. In half of the studied cases, we have indeed found a quite significant increase of the simulated precipitation. When the atmospheric layer containing aerosol is sufficiently moist, the warming caused by the interaction between aerosol and radiation increases the potential instability despite the reduced dynamical forcing due to the weakening of the convergence, finally resulting in an increase of precipitation. In conclusion, while the heavy precipitation events over Liguria region are triggered by the
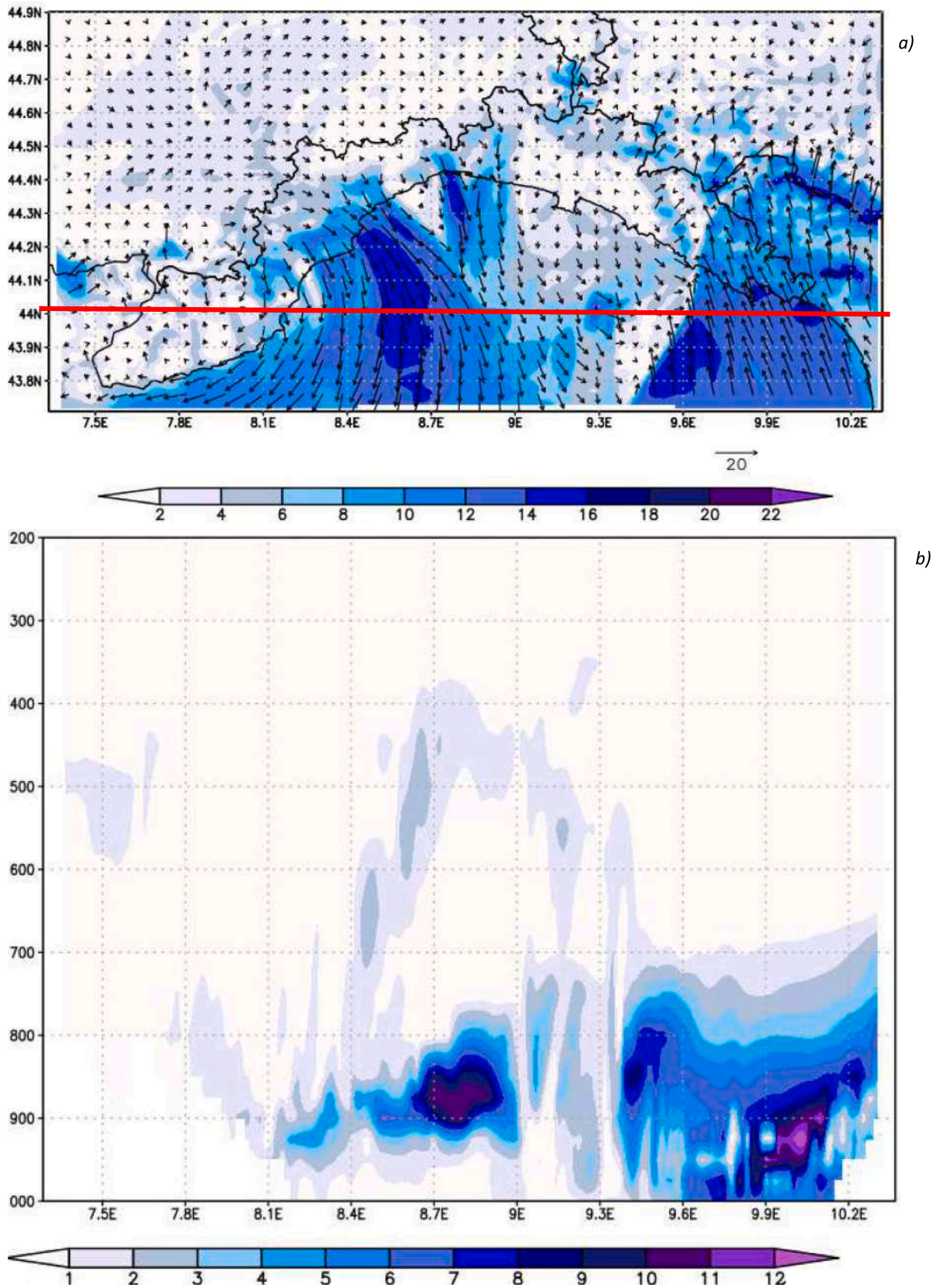
**Fig. 11.** Panel *a*): 10 m wind field simulated at 15 UTC of 25 October 2011 by simulation fully_cpl. Panel *b*): OIN (unit: µg kg$^{-1}$-dry air) vertical cross section, referring to 15 UTC of 25 October 2011, simulated by run fully_cpl. The vertical cross section is taken at 44°N, in correspondence with the red line present in the panel *a*). (For interpretation of the references to colour in this figure legend, the reader is referred to the web version of this article.)
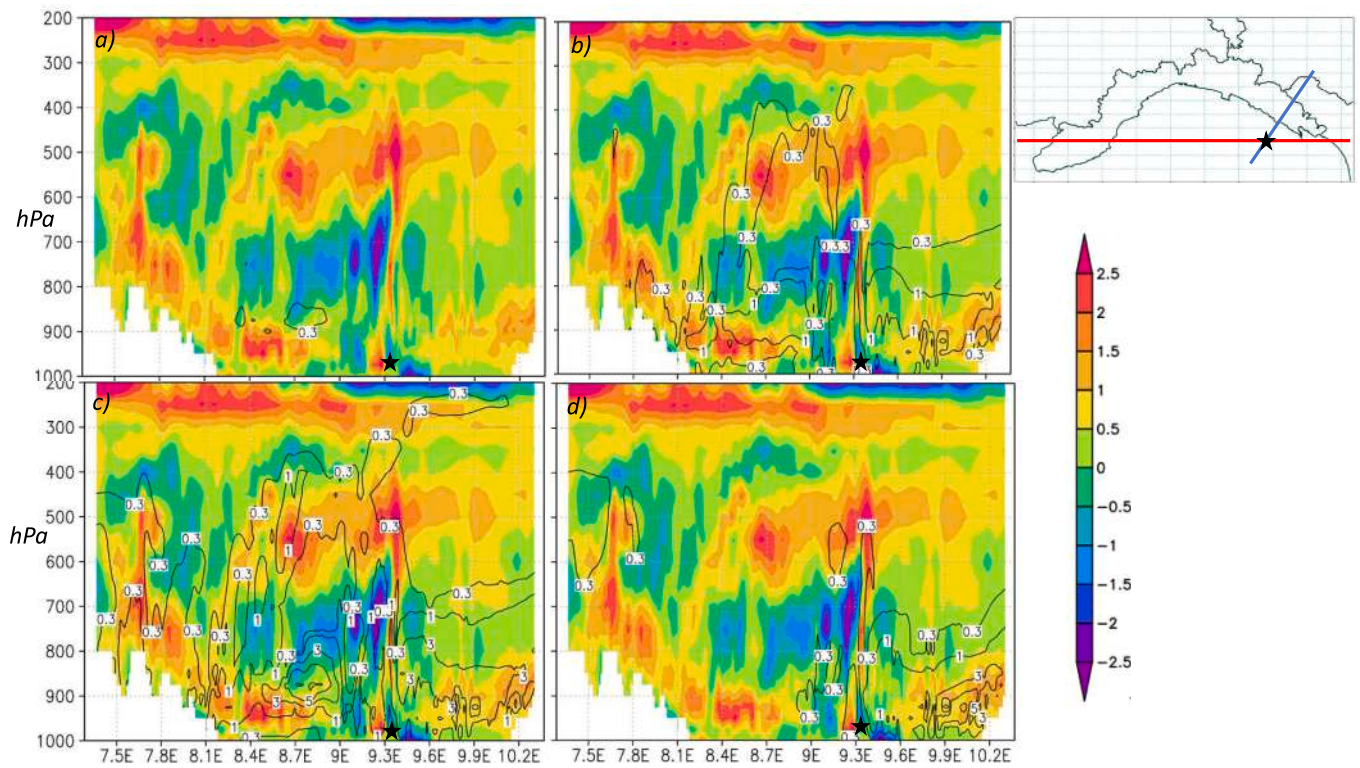
**Fig. 12.** OIN (contours, unit: μg kg$^{-1}$-dry air) vertical cross section, referring to 15 UTC of 25 October 2011, simulated by run fully_cpl for the four different size bins taken into account by MOSAIC: dry diameters of 0.039–0.156 μm, panel a), 0.156–0.625 μm, panel b), 0.625–2.500 μm, panel c) and 2.5–10.0 μm, panel d). Shaded contour represents the vertical cross section of temperature difference (unit: K) between simulations fully_cpl and ctrl_run. The vertical cross section is taken at 44° N, in correspondence with the red line present in the small panel in the upper-right corner, while the black star identifies the intersection between the vertical cross section position and the convergence line. (For interpretation of the references to colour in this figure legend, the reader is referred to the web version of this article.)
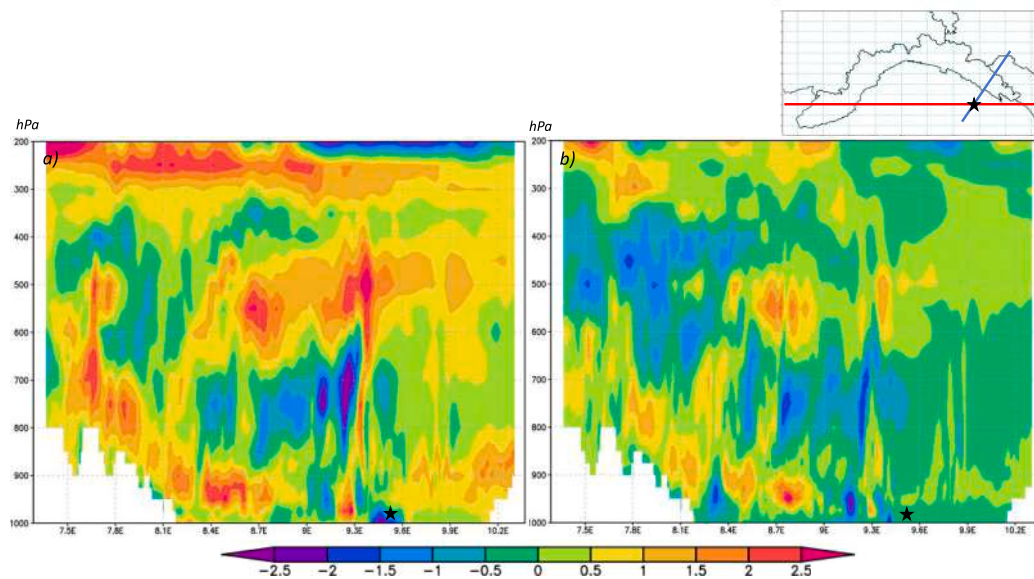


**Fig. 13.** Vertical cross section of temperature difference (unit: K) between fully_cpl and ctrl_run, panel a), and between MP_fdb and ctrl_run, panel b). The vertical cross section, taken at 44° N (red line present in the small panel in the upper-right corner), refers to 15 UTC of 25 October 2011. The blue line in the small panel in the upper-right corner identifies the position of the convergence line and the black star (reported also in panel a) and b)) identifies the intersection between the convergence line and the latitude along which the cross section has been extracted. (For interpretation of the references to colour in this figure legend, the reader is referred to the web version of this article.)

convergence line, in agreement with the mechanism illustrated above, they are the result of a multi-scale interaction where also the orography (both at local and large-scale) can trigger precipitation inland and can

make the interpretation of the development mechanisms more tricky. Thus, the role of the aerosol in modulating these different contributions can be difficult to disentangle and, anyway, out of the scope of the
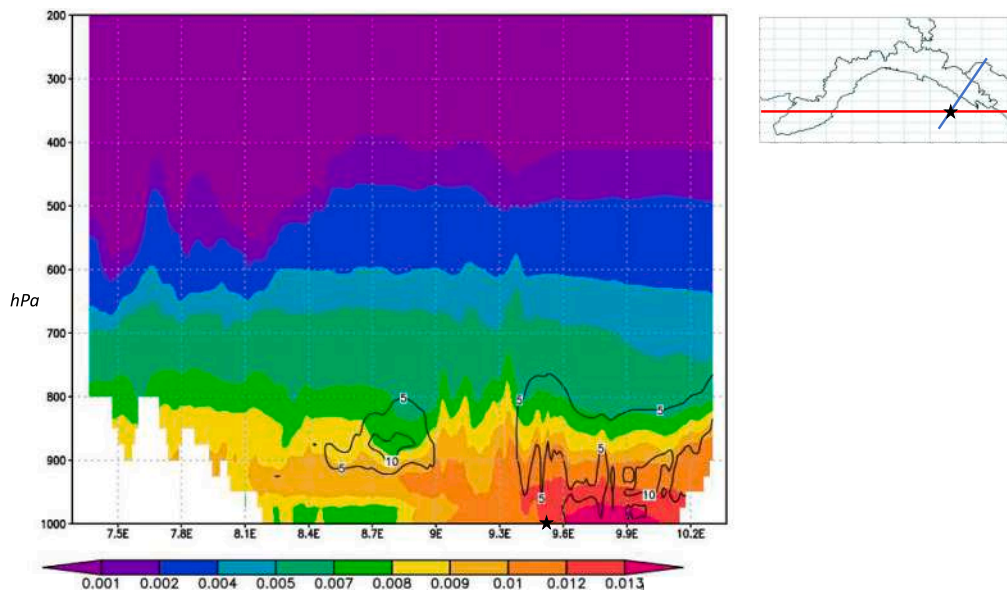
**Fig. 14.** OIN (contour, unit: $\mu g\ kg^{-1}$-dry air) vertical cross section, taken at 44° N (red line present in the small panel in the upper-right corner), overlapped to the water vapor mixing ratio vertical cross section (shaded contour, unit: $kg\ kg^{-1}$). Plot refers to 15 UTC of 25 October 2011 of the simulation fully_cpl. The blue line in the small panel in the upper-right corner identifies the position of the convergence line and the black star (reported also in the main panel) identifies the intersection between the convergence line and the latitude along which the cross section has been extracted. (For interpretation of the references to colour in this figure legend, the reader is referred to the web version of this article.)
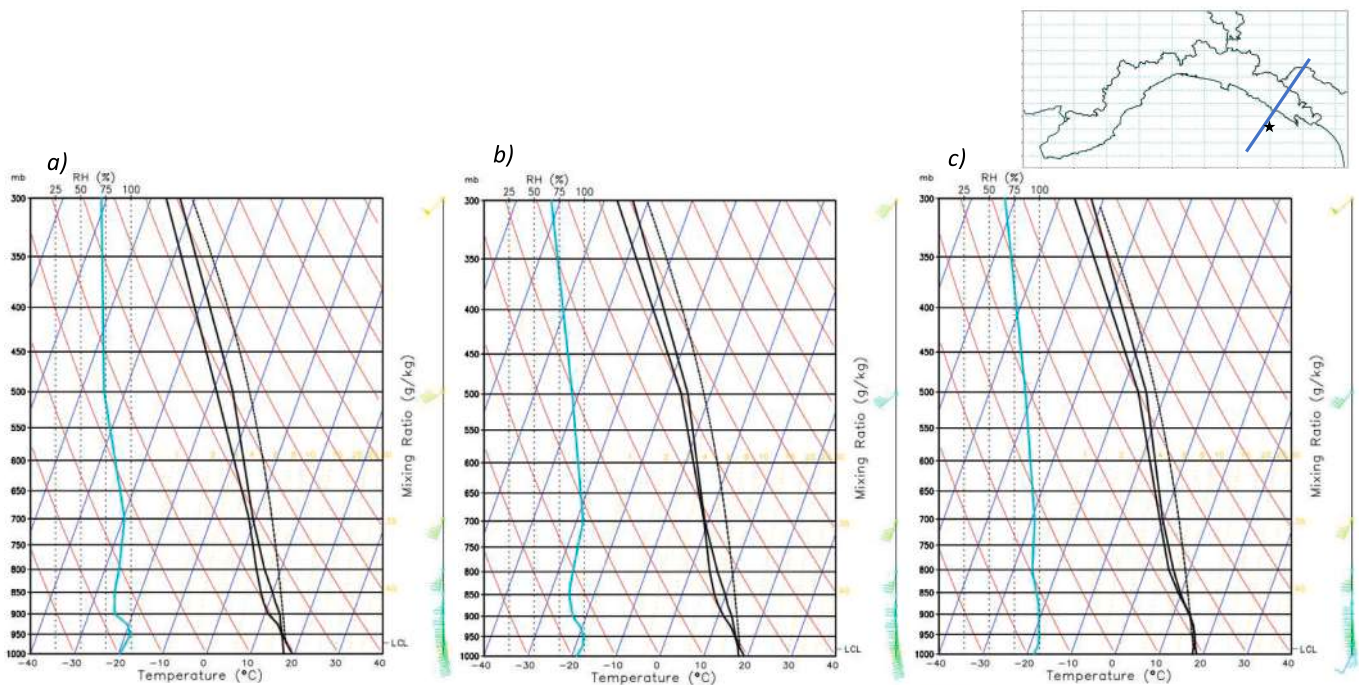


**Fig. 15.** Simulated soundings extracted at 44.15° N and 9.6° E for simulations ctrl_run, panel a), MP_fdb, panel b) and fully_cpl, panel c), at 09 UTC of 25 October 2011. Black star in the upper-right corner indicates the position of the simulated sounding, while the blue line identifies the position of the convergence line. (For interpretation of the references to colour in this figure legend, the reader is referred to the web version of this article.)

present paper.

**CRediT authorship contribution statement**

**Francesco Ferrari:** Writing – original draft, Software, Methodology, Formal analysis, Data curation, Conceptualization. **Umberto Rizza:** Writing – review & editing, Methodology, Data curation, Conceptualization. **Mauro Morichetti:** Writing – review & editing, Methodology,

Data curation, Conceptualization. **Federico Cassola:** Data curation, Conceptualization, Methodology, Writing – review & editing. **Mario Marcello Miglietta:** Conceptualization, Data curation, Methodology, Writing – review & editing. **Andrea Mazzino:** Writing – review & editing, Methodology, Data curation, Conceptualization.

## Declaration of competing interest

The authors declare that they have no known competing financial interests or personal relationships that could have appeared to influence the work reported in this paper.

## Data availability

Data will be made available on request.

## Acknowledgement

## References

Baró, R., Jiménez-Guerrero, P., Balzarini, A., Curci, G., Forkel, R., Grell, G., Hirtl, M., Honzak, L., Langer, M., Pérez, J.L., Pirovano, G., San José, R., Tuccella, P., Werhahn, J., Žabkar, R., 2015. Sensitivity analysis of the microphysics scheme in wrf-chem contributions to aqmeii phase 2. Atmos. Environ. 115, 620–629. URL: https://www.sciencedirect.com/science/article/pii/S1352231015000709 https://doi.org/10.1016/j.atmosenv.2015.01.047.

Bougeault, P., Binder, P., Buzzi, A., Dirks, R., Houze, R., Kuettner, J., Smith, R.B., Steinacker, R., Volkert, H., 2001. The map special observing period. Bull. Am. Meteorol. Soc. 82, 433–462.

Buzzi, A., Davolio, S., Malguzzi, P., Drofa, O., Mastrangelo, D., 2014. Heavy rainfall episodes over Liguria of autumn 2011: numerical forecasting experiments. Nat. Hazards Earth Syst. Sci. 14, 1325–1340.

Cassola, F., Ferrari, F., Mazzino, A., 2015. Numerical simulations of mediterranean heavy precipitation events with the WRF model: a verification exercise using different approaches. Atmos. Res. 164–165, 3–18.

Cassola, F., Ferrari, F., Mazzino, A., Miglietta, M.M., 2016. The role of the sea on the flash floods events over Liguria (northwestern Italy). Geophys. Res. Lett. 43, 3534–3542.

Cassola, F., Iengo, A., Turato, B., 2023. Extreme convective precipitation in Liguria (Italy): a brief description and analysis of the event occurred on october 4, 2021. Bulletin of Atmospheric. Sci. Technol. 4.

Cavaleri, L., Barbariol, F., Bertotti, L., Besio, G., Ferrari, F., 2022. The 29 october 2018 storm in northern Italy: its multiple actions in the ligurian sea. Prog. Oceanogr. 201, 102715 https://doi.org/10.1016/j.pocean.2021.102715.

Chaibou, A., Aziz, A., Ma, X., Sha, T., 2020. Dust radiative forcing and its impact on surface energy budget over west africa. Sci. Rep. 10, 12236.

Charlson, R.J., Schwartz, S.E., Hales, J.M., Cess, R.D., Coakley, J.A., Hansen, J.E., Hofmann, D.J., 1992. Climate forcing by anthropogenic aerosols. Science 255, 423–430. https://doi.org/10.1126/science.255.5043.423.

Chen, F., Dudhia, J., 2001. Coupling an advanced land-surface/hydrology model with the Penn state/NCAR MM5 modeling system. Part I: model description and implementation. Mon. Weather Rev. 12, 569–585.

Clough, S., Shephard, M., Mlawer, E., Delamere, J., Iacono, M., Cady-Pereira, K., Boukabara, S., Brown, P., 2005. Atmospheric radiative transfer modeling: a summary of the aer codes. J. Quant. Spectrosc. Radiat. Transf. 91, 233–244. https://doi.org/10.1016/j.jqsrt.2004.05.058.

Davolio, S., Silvestro, F., Malguzzi, P., 2015. Effects of increasing horizontal resolution in a convection permitting model on flood forecasting: the 2011 dramatic events in Liguria (Italy). J. Hydrometeorol. 16, 1843–1856.

Drobinski, P., Ducrocq, V., Alpert, P., Anagnostou, E., Beranger, K., Borga, M., Braud, I., Chanzy, A., Davolio, S., Delrieu, G., Estournel, C., Filali Boubrahmi, N., Font, J., Grubisic, V., Gualdi, S., Homar, V., Ivancan-Picek, B., Kottmeier, C., Kotroni, V., Lagouvardos, K., Lionello, P., Llasat, M.C., Ludwig, W., Lutoff, C., Mariotti, A., Richard, E., Romero, R., Rotunno, R., Roussot, O., Ruin, I., Somot, S., Taupier-Letage, I., Tintor, J., Uijlenhoet, R., Wernli, H., 2014. HyMeX: a 10-year multidisciplinary program on the Mediterranean water cycle. Bull. Am. Meteorol. Soc. 95, 1063–1082. https://doi.org/10.1175/BAMS-D-12-00242.1.

Duan, Y., Petters, M.D., Barros, A.P., 2019. Understanding aerosol–cloud interactions through modeling the development of orographic cumulus congestus during iphex. Atmos. Chem. Phys. 19, 1413–1437. URL: https://acp.copernicus.org/articles/19/1413/2019/ https://doi.org/10.5194/acp-19-1413-2019.

Emmons, L.K., Walters, S., Hess, P.G., Lamarque, J.-F., Pfister, G.G., Fillmore, D., Granier, C., Guenther, A., Kinnison, D., Laepple, T., Orlando, J., Tie, X., Tyndall, G., Wiedinmyer, C., Baughcum, S.L., Kloster, S., 2009. Description and evaluation of the model for ozone and related chemical tracers, version 4 (mozart-4). Geosci. Model Dev. Discuss. 3 https://doi.org/10.5194/gmd-3-43-2010.

Fast, J.D., Gustafson Jr., W.I., Easter, R.C., Zaveri, R.A., Barnard, J.C., Chapman, E.G., Grell, G.A., Peckham, S.E., 2006. Evolution of ozone, particulates, and aerosol direct radiative forcing in the vicinity of Houston using a fully coupled meteorology-chemistry-aerosol model. J. Geophys. Res. Atmos. 111.

Ferrari, F., Cassola, F., Tuju, P.E., Stocchino, A., Brotto, P., Mazzino, A., 2020. Impact of model resolution and initial/boundary conditions in forecasting flood-causing precipitations. Atmosphere 11, 592.

Ferrari, F., Cassola, F., Tuju, P., Mazzino, A., 2021. RANS and LES face to face for forecasting extreme precipitation events in the Liguria region (northwestern Italy). Atmos. Res. 259, 105654. URL: https://www.sciencedirect.com/science/article/pii/S0169809521002064 https://doi.org/10.1016/j.atmosres.2021.105654.

Fiori, E., Commellas, A., Molini, L., Rebora, N., Siccardi, F., Gochis, D.J., Tanelli, S., Parodi, A., 2014. Analysis and hindcast simulation of an extreme rainfall event in the Mediterranean area: the Genoa 2011 case. Atmos. Res. 138, 13–29.

Gascon, E., Laviola, S., Merino, A., Miglietta, M., 2016. Analysis of a localized flash-flood event over the central mediterranean. Atmos. Res. 182, 256–268. https://doi.org/10.1016/j.atmosres.2016.08.007.

Gelaro, R., McCarty, W., Suárez, M.J., Todling, R., Molod, A., Takacs, L., Randles, C.A., Darmenov, A., Bosilovich, M.G., Reichle, R., Wargan, K., Coy, L., Cullather, R., Draper, C., Akella, S., Buchard, V., Conaty, A., da Silva, A.M., Gu, W., Kim, G.K., Koster, R., Lucchesi, R., Merkova, D., Nielsen, J.E., Partyka, G., Pawson, S., Putman, W., Rienecker, M., Schubert, S.D., Sienkiewicz, M., Zhao, B., 2017. The modern-era retrospective analysis for research and applications, version 2 (merra-2). J. Clim. 30, 5419–5454. URL: https://journals.ametsoc.org/view/journals/clim/30/14/jcli-d-16-0758.1.xml https://doi.org/10.1175/JCLI-D-16-0758.1.

Goudie, A., Middleton, N., 2001. Saharan dust storms: nature and consequences. Earth Sci. Rev. 56, 179–204. https://doi.org/10.1016/S0012-8252(01)00067-8.

Grell, G.A., Freitas, S.R., 2014. A scale and aerosol aware stochastic convective parameterization for weather and air quality modeling. Atmos. Chem. Phys. 14, 5233–5250. URL: https://acp.copernicus.org/articles/14/5233/2014/ https://doi.org/10.5194/acp-14-5233-2014.

Grell, G.A., Peckham, S.E., Schmitz, R., McKeen, S.A., Frost, G., Skamarock, W.C., Eder, B., 2005. Fully coupled "online" chemistry within the wrf model. Atmos. Environ. 39, 6957–6975. URL: https://www.sciencedirect.com/science/article/pii/S1352231005003560 https://doi.org/10.1016/j.atmosenv.2005.04.027.

Hong, S.Y., Noh, Y., Dudhia, J., 2006. A new vertical diffusion package with an explicit treatment of entrainment processes. Mon. Weather Rev. 134, 2318–2341. https://doi.org/10.1175/MWR3199.1.

Huang, J., Wang, T., Wang, W., Li, Z., Yan, H., 2014. Climate effects of dust aerosols over east asian arid and semiarid regions. J. Geophys. Res. Atmos. 119 https://doi.org/10.1002/2014JD021796, 11,398–11,416.

Iacono, M.J., Delamere, J.S., Mlawer, E.J., Shephard, M.W., Clough, S.A., Collins, W.D., 2008. Radiative forcing by long-lived greenhouse gases: calculations with the aer radiative transfer models. J. Geophys. Res. Atmos. 113 https://doi.org/10.1029/2008JD009944.

Jimenez, P.A., Dudhia, J., González-Rouco, J.F., Navarro, J., Montávez, J.P., García-Bustamante, E., 2012. A revised scheme for the wrf surface layer formulation. Mon. Weather Rev. 140, 170–181.

Juda-Rezler, K., Reizer, M., Maciejewska, K., Błaszczak, B., Klejnowski, K., 2020. Characterization of atmospheric pm2.5 sources at a central european urban background site. Sci. Total Environ. 713, 136729. URL: https://www.sciencedirect.com/science/article/pii/S0048969720302394 https://doi.org/10.1016/j.scitotenv.2020.136729.

Kiehl, J.T., Briegleb, B.P., 1993. The relative roles of sulfate aerosols and greenhouse gases in climate forcing. Science 260, 311–314. https://doi.org/10.1126/science.260.5106.311.

Knote, C., Hodzic, A., Jimenez, J.L., 2015. The effect of dry and wet deposition of condensable vapors on secondary organic aerosols concentrations over the continental us. Atmos. Chem. Phys. 15, 1–18. URL: https://acp.copernicus.org/articles/15/1/2015/ https://doi.org/10.5194/acp-15-1-2015.

Kumar, R., Barth, M.C., Pfister, G.G., Naja, M., Brasseur, G.P., 2014. Wrf-chem simulations of a typical pre-monsoon dust storm in northern India: influences on aerosol optical properties and radiation budget. Atmos. Chem. Phys. 14, 2431–2446. URL: https://acp.copernicus.org/articles/14/2431/2014/ https://doi.org/10.5194/acp-14-2431-2014.

Levin, Z., Cotton, W., 2009. Summary. Springer, Netherlands, pp. 295–300.

Liu, Y., Zhu, Q., Hua, S., Alam, K., Dai, T., Cheng, Y., 2020. Tibetan plateau driven impact of taklimakan dust on northern rainfall. Atmos. Environ. 234, 117583. URL: https://www.sciencedirect.com/science/article/pii/S1352231020303174 https://doi.org/10.1016/j.atmosenv.2020.117583.

Liu, Y., Huang, J., Wang, T., Li, J., Yan, H., He, Y., 2022. Aerosol-cloud interactions over the tibetan plateau: an overview. Earth Sci. Rev. 234, 104216. URL: https://www.sciencedirect.com/science/article/pii/S0012825222003002 https://doi.org/10.1016/j.earscirev.2022.104216.

Mamun, A., Chen, Y., Liang, J., 2021. Radiative and cloud microphysical effects of the saharan dust simulated by the wrf-chem model. J. Atmos. Sol. Terr. Phys. 219, 105646. URL: https://www.sciencedirect.com/science/article/pii/S1364682621001057 https://doi.org/10.1016/j.jastp.2021.105646.

Marenco, F., Bonasoni, P., Calzolari, F., Ceriani, M., Chiari, M., Cristofanelli, P., D'Alessandro, A., Fermo, P., Lucarelli, F., Mazzei, F., Nava, S., Piazzalunga, A., Prati, P., Valli, G., Vecchi, R., 2006. Characterization of atmospheric aerosols at monte cimone, italy, during summer 2004: Source apportionment and transport mechanisms. J. Geophys. Res. Atmos. 111 https://doi.org/10.1029/2006JD007145.

Miglietta, M.M., Davolio, S., 2022. Dynamical forcings in heavy precipitation events over Italy: lessons from the hymex sop1 campaign. Hydrol. Earth Syst. Sci. 26, 627–646. URL: https://hess.copernicus.org/articles/26/627/2022/ https://doi.org/10.5194/hess-26-627-2022.

Miglietta, M.M., Regano, A., 2008. An observational and numerical study of a flash-flood event over South-Eastern Italy. Nat. Hazards Earth Syst. Sci. 8, 1417–1430. URL: https://nhess.copernicus.org/articles/8/1417/2008/ https://doi.org/10.5194/nhess-8-1417-2008.

Morrison, H., Thompson, G., Tatarskii, V., 2009. Impact of cloud microphysics on the development of trailing stratiform precipitation in a simulated squall line: comparison of one- and two-moment schemes. Mon. Weather Rev. 137, 991–1007.

Panicker, A.S., Pandithurai, G., Safai, P.D., Kewat, S., 2008. Observations of enhanced aerosol longwave radiative forcing over an urban environment. Geophys. Res. Lett. 35 https://doi.org/10.1029/2007GL032879.

Park, J.M., van den Heever, S.C., 2022. Weakening of tropical sea breeze convective systems through interactions of aerosol, radiation, and soil moisture. Atmos. Chem. Phys. 22, 10527–10549. URL: https://acp.copernicus.org/articles/22/10527/2022/ https://doi.org/10.5194/acp-22-10527-2022.

Rebora, N., Molini, L., Casella, E., Commellas, A., Fiori, E., Pignone, F., Siccardi, F., Silvestro, F., Tanelli, S., Parodi, A., 2013. Extreme rainfall in the Mediterranean: what can we learn from observations? J. Hydrometeorol. 14, 906–922.

Rizza, U., Barnaba, F., Miglietta, M.M., Mangia, C., Di Liberto, L., Dionisi, D., Costabile, F., Grasso, F., Gobbi, G.P., 2017. Wrf-chem model simulations of a dust outbreak over the central mediterranean and comparison with multi-sensor desert dust observations. Atmos. Chem. Phys. 17, 93–115. https://acp.copernicus.org/articles/17/93/2017/. https://doi.org/10.5194/acp-17-93-2017.

Rizza, U., Canepa, E., Miglietta, M.M., Passerini, G., Morichetti, M., Mancinelli, E., Virgili, S., Besio, G., De Leo, F., Mazzino, A., 2021. Evaluation of drag coefficients under medicane conditions: Coupling waves, sea spray and surface friction. Atmos. Res. 247, 105207.

Rizza, U., Avolio, E., Morichetti, M., Di Liberto, L., Bellini, A., Barnaba, F., Virgili, S., Passerini, G., Mancinelli, E., 2023. On the interplay between desert dust and meteorology based on wrf-chem simulations and remote sensing observations in the mediterranean basin. Remote Sens. 15 https://doi.org/10.3390/rs15020435 https://www.mdpi.com/2072-4292/15/2/435.

Satheesh, S.K., Lubin, D., 2003. Short wave versus long wave radiative forcing by indian ocean aerosols: Role of sea-surface winds. Geophys. Res. Lett. 30 https://doi.org/10.1029/2003GL017499.

Silvestro, F., Rebora, N., Giannoni, F., Cavallo, A., Ferraris, L., 2016. The flash flood of the Bisagno Creek on 9th October 2014: an "unfortunate" combination of spatial and temporal scales. J. Hydrol. 541, 50–62. URL: http://www.sciencedirect.com/science/article/pii/S0022169415005636 https://doi.org/10.1016/j.jhydrol.2015.08.004 (flash floods, hydro-geomorphic response and risk management).

Tao, W.K., Chen, J.P., Li, Z., Wang, C., Zhang, C., 2012. Impact of aerosols on convective clouds and precipitation. Rev. Geophys. 50 https://doi.org/10.1029/2011RG000369.

Twomey, S., 1974. Pollution and the planetary albedo. Atmos. Environ. 1967 (8), 1251–1256. https://doi.org/10.1016/0004-6981(74)90004-3.

Twomey, S., 1991. Aerosols, clouds and radiation. Atmos. Environ. Part A 25, 2435–2442. https://doi.org/10.1016/0960-1686(91)90159-5. symposium on Global Climatic Effects of Aerosols.

Ukhov, A., Ahmadov, R., Grell, G., Stenchikov, G., 2021. Improving dust simulations in wrf-chem v4.1.3 coupled with the gocart aerosol module. Geosci. Model Dev. 14, 473–493. https://gmd.copernicus.org/articles/14/473/2021/. https://doi.org/10.5194/gmd-14-473-2021.

Wackernagel, H., 1995. Ordinary Kriging. Springer, Berlin Heidelberg, pp. 74–81.

Xie, S., Liu, X., Zhao, C., Zhang, Y., 2013. Sensitivity of cam5-simulated arctic clouds and radiation to ice nucleation parameterization. J. Clim. 26, 5981–5999. URL: https://journals.ametsoc.org/view/journals/clim/26/16/jcli-d-12-00517.1.xml https://doi.org/10.1175/JCLI-D-12-00517.1.

Zaveri, R.A., Easter, R.C., Fast, J.D., Peters, L.K., 2008. Model for simulating aerosol interactions and chemistry (mosaic). J. Geophys. Res. Atmos. 113 https://doi.org/10.1029/2007JD008782.

Zhang, B., Wang, Y., Hao, J., 2015. Simulating aerosol–radiation–cloud feedbacks on meteorology and air quality over eastern China under severe haze conditionsin winter. Atmos. Chem. Phys. 15, 2387–2404.